

## Coherent backscattering in the cross-polarized channel

Michael I. Mishchenko<sup>1,\*</sup> and Daniel W. Mackowski<sup>2</sup>

<sup>1</sup>*NASA Goddard Institute for Space Studies, 2880 Broadway, New York, New York 10025, USA*

<sup>2</sup>*Department of Mechanical Engineering, Auburn University, Alabama 36849, USA*

(Received 22 November 2010; published 31 January 2011)

We analyze the asymptotic behavior of the cross-polarized enhancement factor in the framework of the standard low-packing-density theory of coherent backscattering by discrete random media composed of spherically symmetric particles. It is shown that if the particles are strongly absorbing or if the smallest optical dimension of the particulate medium (i.e., the optical thickness of a plane-parallel slab or the optical diameter of a spherically symmetric volume) approaches zero, then the cross-polarized enhancement factor tends to its upper-limit value 2. This theoretical prediction is illustrated using direct computer solutions of the Maxwell equations for spherical volumes of discrete random medium.

DOI: [10.1103/PhysRevA.83.013829](https://doi.org/10.1103/PhysRevA.83.013829)

PACS number(s): 42.25.Bs, 42.25.Dd, 42.25.Fx, 42.25.Hz

### I. INTRODUCTION

Coherent backscattering (CB) of light (otherwise known as weak localization of electromagnetic waves) is a remarkable interference effect surviving any degree of disorder of a sparse particulate medium [1–6]. Although CB has been studied extensively over the past 25 years, some aspects of this phenomenon remain poorly understood and require further analysis. One of the puzzling quantitative characteristics of CB is the so-called cross-polarized enhancement factor  $\zeta_{\perp,\parallel}$ . In early laboratory experiments (e.g., [7,8]), the  $\zeta_{\perp,\parallel}$  values measured for optically thick (essentially semi-infinite) particulate layers were found to be much closer to unity than those of the copolarized enhancement factor  $\zeta_{\parallel,\parallel}$ . Yet numerically exact theoretical results valid in the asymptotic limit of very small packing density revealed frequent occurrences of  $\zeta_{\perp,\parallel}$  values close to the theoretical upper limit  $\zeta_{\perp,\parallel}^{\max} = 2$  [5]. Most intriguingly, these large values of  $\zeta_{\perp,\parallel}$  were found for optically thin particulate slabs or for strongly absorbing particles, that is, in cases when the amount of multiple scattering is minimized and many other manifestations of CB are suppressed.

In this paper, we give a simple physical explanation of this behavior of the cross-polarized enhancement factor. Furthermore, we show that this behavior is reproduced not only by the asymptotic low-density theory of CB but also by direct computer solutions of the macroscopic Maxwell equations for spherical volumes of discrete random media.

### II. THEORY

In the framework of the standard low-density theory of radiative transfer and CB [5], the response of a discrete

random medium to external illumination in the form of a plane electromagnetic wave or a parallel quasimonochromatic beam of light is fully described by the corresponding  $4 \times 4$  real-valued Mueller matrix  $\mathbf{R}$ :

$$\begin{pmatrix} I^{\text{sca}}(\hat{\mathbf{n}}^{\text{sca}}) \\ Q^{\text{sca}}(\hat{\mathbf{n}}^{\text{sca}}) \\ U^{\text{sca}}(\hat{\mathbf{n}}^{\text{sca}}) \\ V^{\text{sca}}(\hat{\mathbf{n}}^{\text{sca}}) \end{pmatrix} \propto \mathbf{R}(\hat{\mathbf{n}}^{\text{sca}}, \hat{\mathbf{n}}^{\text{inc}}) \begin{pmatrix} I^{\text{inc}} \\ Q^{\text{inc}} \\ U^{\text{inc}} \\ V^{\text{inc}} \end{pmatrix}. \quad (1)$$

Here, the Stokes parameters  $I$ ,  $Q$ ,  $U$ , and  $V$  of the incident (“inc”) and scattered (“sca”) light are defined with respect to the scattering plane, that is, the plane defined by the unit vectors of the incidence,  $\hat{\mathbf{n}}^{\text{inc}}$ , and scattering,  $\hat{\mathbf{n}}^{\text{sca}}$ , directions (Fig. 1). The Mueller matrix is decomposed into the first-order scattering (superscript 1), diffuse multiple-scattering (superscript  $M$ ), and cyclical (superscript  $C$ ) contributions [9–14]:

$$\mathbf{R}(\hat{\mathbf{n}}^{\text{sca}}, \hat{\mathbf{n}}^{\text{inc}}) = \mathbf{R}^1(\hat{\mathbf{n}}^{\text{sca}}, \hat{\mathbf{n}}^{\text{inc}}) + \mathbf{R}^M(\hat{\mathbf{n}}^{\text{sca}}, \hat{\mathbf{n}}^{\text{inc}}) + \mathbf{R}^C(\hat{\mathbf{n}}^{\text{sca}}, \hat{\mathbf{n}}^{\text{inc}}). \quad (2)$$

Both  $\mathbf{R}^1(\hat{\mathbf{n}}^{\text{sca}}, \hat{\mathbf{n}}^{\text{inc}})$  and  $\mathbf{R}^M(\hat{\mathbf{n}}^{\text{sca}}, \hat{\mathbf{n}}^{\text{inc}})$  can be found by solving the standard vector radiative transfer equation [5]. Furthermore, in the case of the exact backscattering direction ( $\hat{\mathbf{n}}^{\text{sca}} = -\hat{\mathbf{n}}^{\text{inc}}$ ), the cyclical Mueller matrix can be rigorously expressed in terms of the diffuse multiple-scattering matrix. Specifically, assuming that the particulate medium is macroscopically isotropic and mirror-symmetric [15] and can be modeled as a plane-parallel slab of infinite horizontal extent or as a spherically symmetric volume, we have [5,16]

$$\mathbf{R}^C(-\hat{\mathbf{n}}^{\text{inc}}, \hat{\mathbf{n}}^{\text{inc}}) = \begin{pmatrix} R_{11}^C(-\hat{\mathbf{n}}^{\text{inc}}, \hat{\mathbf{n}}^{\text{inc}}) & R_{12}^M(-\hat{\mathbf{n}}^{\text{inc}}, \hat{\mathbf{n}}^{\text{inc}}) & 0 & 0 \\ R_{12}^M(-\hat{\mathbf{n}}^{\text{inc}}, \hat{\mathbf{n}}^{\text{inc}}) & R_{22}^C(-\hat{\mathbf{n}}^{\text{inc}}, \hat{\mathbf{n}}^{\text{inc}}) & 0 & 0 \\ 0 & 0 & R_{33}^C(-\hat{\mathbf{n}}^{\text{inc}}, \hat{\mathbf{n}}^{\text{inc}}) & R_{34}^M(-\hat{\mathbf{n}}^{\text{inc}}, \hat{\mathbf{n}}^{\text{inc}}) \\ 0 & 0 & -R_{34}^M(-\hat{\mathbf{n}}^{\text{inc}}, \hat{\mathbf{n}}^{\text{inc}}) & R_{44}^C(-\hat{\mathbf{n}}^{\text{inc}}, \hat{\mathbf{n}}^{\text{inc}}) \end{pmatrix}, \quad (3)$$

where

$$R_{11}^C(-\hat{\mathbf{n}}^{\text{inc}}, \hat{\mathbf{n}}^{\text{inc}}) = \frac{1}{2} [R_{11}^M(-\hat{\mathbf{n}}^{\text{inc}}, \hat{\mathbf{n}}^{\text{inc}}) + R_{22}^M(-\hat{\mathbf{n}}^{\text{inc}}, \hat{\mathbf{n}}^{\text{inc}}) - R_{33}^M(-\hat{\mathbf{n}}^{\text{inc}}, \hat{\mathbf{n}}^{\text{inc}}) + R_{44}^M(-\hat{\mathbf{n}}^{\text{inc}}, \hat{\mathbf{n}}^{\text{inc}})], \quad (4)$$

\*mmishchenko@giss.nasa.gov

$$R_{22}^C(-\hat{\mathbf{n}}^{\text{inc}}, \hat{\mathbf{n}}^{\text{inc}}) = \frac{1}{2} [R_{11}^M(-\hat{\mathbf{n}}^{\text{inc}}, \hat{\mathbf{n}}^{\text{inc}}) + R_{22}^M(-\hat{\mathbf{n}}^{\text{inc}}, \hat{\mathbf{n}}^{\text{inc}}) + R_{33}^M(-\hat{\mathbf{n}}^{\text{inc}}, \hat{\mathbf{n}}^{\text{inc}}) - R_{44}^M(-\hat{\mathbf{n}}^{\text{inc}}, \hat{\mathbf{n}}^{\text{inc}})], \quad (5)$$

$$R_{44}^C(-\hat{\mathbf{n}}^{\text{inc}}, \hat{\mathbf{n}}^{\text{inc}}) = \frac{1}{2} [R_{11}^M(-\hat{\mathbf{n}}^{\text{inc}}, \hat{\mathbf{n}}^{\text{inc}}) - R_{22}^M(-\hat{\mathbf{n}}^{\text{inc}}, \hat{\mathbf{n}}^{\text{inc}}) + R_{33}^M(-\hat{\mathbf{n}}^{\text{inc}}, \hat{\mathbf{n}}^{\text{inc}}) + R_{44}^M(-\hat{\mathbf{n}}^{\text{inc}}, \hat{\mathbf{n}}^{\text{inc}})]. \quad (7)$$

$$R_{33}^C(-\hat{\mathbf{n}}^{\text{inc}}, \hat{\mathbf{n}}^{\text{inc}}) = \frac{1}{2} [-R_{11}^M(-\hat{\mathbf{n}}^{\text{inc}}, \hat{\mathbf{n}}^{\text{inc}}) + R_{22}^M(-\hat{\mathbf{n}}^{\text{inc}}, \hat{\mathbf{n}}^{\text{inc}}) + R_{33}^M(-\hat{\mathbf{n}}^{\text{inc}}, \hat{\mathbf{n}}^{\text{inc}}) + R_{44}^M(-\hat{\mathbf{n}}^{\text{inc}}, \hat{\mathbf{n}}^{\text{inc}})], \quad (6)$$

Note that the matrices  $\mathbf{R}^1(-\hat{\mathbf{n}}^{\text{inc}}, \hat{\mathbf{n}}^{\text{inc}})$  and  $\mathbf{R}^M(-\hat{\mathbf{n}}^{\text{inc}}, \hat{\mathbf{n}}^{\text{inc}})$  have the same block-diagonal structure, with only six independent elements:

$$\mathbf{R}^1(-\hat{\mathbf{n}}^{\text{inc}}, \hat{\mathbf{n}}^{\text{inc}}) = \begin{pmatrix} R_{11}^1(-\hat{\mathbf{n}}^{\text{inc}}, \hat{\mathbf{n}}^{\text{inc}}) & R_{12}^1(-\hat{\mathbf{n}}^{\text{inc}}, \hat{\mathbf{n}}^{\text{inc}}) & 0 & 0 \\ R_{12}^1(-\hat{\mathbf{n}}^{\text{inc}}, \hat{\mathbf{n}}^{\text{inc}}) & R_{22}^1(-\hat{\mathbf{n}}^{\text{inc}}, \hat{\mathbf{n}}^{\text{inc}}) & 0 & 0 \\ 0 & 0 & R_{33}^1(-\hat{\mathbf{n}}^{\text{inc}}, \hat{\mathbf{n}}^{\text{inc}}) & R_{34}^1(-\hat{\mathbf{n}}^{\text{inc}}, \hat{\mathbf{n}}^{\text{inc}}) \\ 0 & 0 & -R_{34}^1(-\hat{\mathbf{n}}^{\text{inc}}, \hat{\mathbf{n}}^{\text{inc}}) & R_{44}^1(-\hat{\mathbf{n}}^{\text{inc}}, \hat{\mathbf{n}}^{\text{inc}}) \end{pmatrix}, \quad (8)$$

$$\mathbf{R}^M(-\hat{\mathbf{n}}^{\text{inc}}, \hat{\mathbf{n}}^{\text{inc}}) = \begin{pmatrix} R_{11}^M(-\hat{\mathbf{n}}^{\text{inc}}, \hat{\mathbf{n}}^{\text{inc}}) & R_{12}^M(-\hat{\mathbf{n}}^{\text{inc}}, \hat{\mathbf{n}}^{\text{inc}}) & 0 & 0 \\ R_{12}^M(-\hat{\mathbf{n}}^{\text{inc}}, \hat{\mathbf{n}}^{\text{inc}}) & R_{22}^M(-\hat{\mathbf{n}}^{\text{inc}}, \hat{\mathbf{n}}^{\text{inc}}) & 0 & 0 \\ 0 & 0 & R_{33}^M(-\hat{\mathbf{n}}^{\text{inc}}, \hat{\mathbf{n}}^{\text{inc}}) & R_{34}^M(-\hat{\mathbf{n}}^{\text{inc}}, \hat{\mathbf{n}}^{\text{inc}}) \\ 0 & 0 & -R_{34}^M(-\hat{\mathbf{n}}^{\text{inc}}, \hat{\mathbf{n}}^{\text{inc}}) & R_{44}^M(-\hat{\mathbf{n}}^{\text{inc}}, \hat{\mathbf{n}}^{\text{inc}}) \end{pmatrix}. \quad (9)$$

The above formulas allow one to introduce the cross-polarized enhancement factor  $\zeta_{\perp, \parallel}$  in the case of incident light linearly polarized in the scattering plane ( $Q^{\text{inc}} = I^{\text{inc}}, U^{\text{inc}} = V^{\text{inc}} = 0$ ). Specifically,  $\zeta_{\perp, \parallel}$  is defined as the ratio of the total cross-polarized intensity (i.e., the total-intensity component polarized perpendicularly to the scattering plane) scattered in the exact backscattering direction to the diffuse cross-polarized intensity. We then have [5]

$$\zeta_{\perp, \parallel}(\hat{\mathbf{n}}^{\text{inc}}) = \frac{I_{\perp}(-\hat{\mathbf{n}}^{\text{inc}})}{I_{\perp}^{\text{diff}}(-\hat{\mathbf{n}}^{\text{inc}})} = \frac{R_{11}^1 - R_{22}^1 + R_{11}^M - R_{22}^M - R_{33}^M + R_{44}^M}{R_{11}^1 - R_{22}^1 + R_{11}^M - R_{22}^M}, \quad (10)$$

where the arguments  $(-\hat{\mathbf{n}}^{\text{inc}}, \hat{\mathbf{n}}^{\text{inc}})$  on the right-hand side are omitted for brevity. Note that in [5] this quantity is denoted as  $\zeta_{\text{hv}}$ . An important property of the cross-polarized enhancement factor is that in the case of spherically symmetric particles  $R_{11}^1(-\hat{\mathbf{n}}^{\text{inc}}, \hat{\mathbf{n}}^{\text{inc}}) \equiv R_{22}^1(-\hat{\mathbf{n}}^{\text{inc}}, \hat{\mathbf{n}}^{\text{inc}})$ , and so the resulting formula for  $\zeta_{\perp, \parallel}$  contains no first-order scattering terms,

$$\zeta_{\perp, \parallel}(\hat{\mathbf{n}}^{\text{inc}}) = \frac{R_{11}^M(-\hat{\mathbf{n}}^{\text{inc}}, \hat{\mathbf{n}}^{\text{inc}}) - R_{22}^M(-\hat{\mathbf{n}}^{\text{inc}}, \hat{\mathbf{n}}^{\text{inc}}) - R_{33}^M(-\hat{\mathbf{n}}^{\text{inc}}, \hat{\mathbf{n}}^{\text{inc}}) + R_{44}^M(-\hat{\mathbf{n}}^{\text{inc}}, \hat{\mathbf{n}}^{\text{inc}})}{R_{11}^M(-\hat{\mathbf{n}}^{\text{inc}}, \hat{\mathbf{n}}^{\text{inc}}) - R_{22}^M(-\hat{\mathbf{n}}^{\text{inc}}, \hat{\mathbf{n}}^{\text{inc}})}. \quad (11)$$

Let us now assume that  $\mathbf{R}^M(-\hat{\mathbf{n}}^{\text{inc}}, \hat{\mathbf{n}}^{\text{inc}})$  is dominated by the diffuse second-order scattering contribution:  $\mathbf{R}^M(-\hat{\mathbf{n}}^{\text{inc}}, \hat{\mathbf{n}}^{\text{inc}}) \approx \mathbf{R}^2(-\hat{\mathbf{n}}^{\text{inc}}, \hat{\mathbf{n}}^{\text{inc}})$ . This is the case when the particles are strongly absorbing, thereby implying a vanishingly small single-scattering albedo  $\omega$ , or when the smallest optical dimension  $T$  of the particulate medium (i.e., the optical thickness of a plane-parallel slab or the optical diameter of a spherically symmetric volume) tends to zero. It is then straightforward to show that in the case of spherically symmetric constituent particles,

$$\lim_{\omega \rightarrow 0} \zeta_{\perp, \parallel}(\hat{\mathbf{n}}^{\text{inc}}) = \lim_{T \rightarrow 0} \zeta_{\perp, \parallel}(\hat{\mathbf{n}}^{\text{inc}}) = 2. \quad (12)$$

Indeed, let us consider an arbitrary second-order scattering ladder diagram involving particles 1 and 2 (Fig. 2). Plane  $B$  contains the centers of the particles, whereas plane  $A$  is the reference plane used to specify the Stokes parameters of the incident and scattered light in Fig. 1. It is clear that to compute the contribution of this diagram to the total diffuse multiple-scattering Mueller matrix, one needs to evaluate the

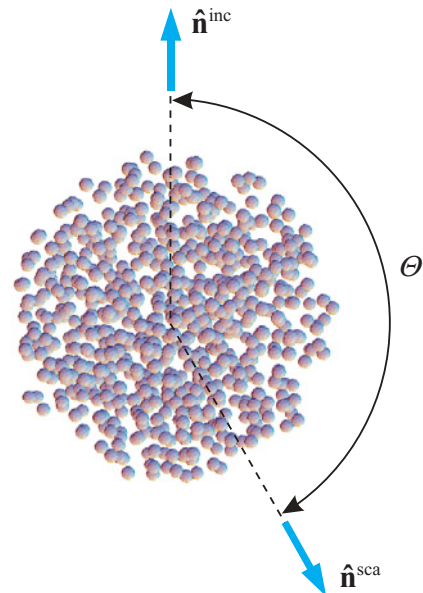


FIG. 1. (Color online) Scattering geometry.

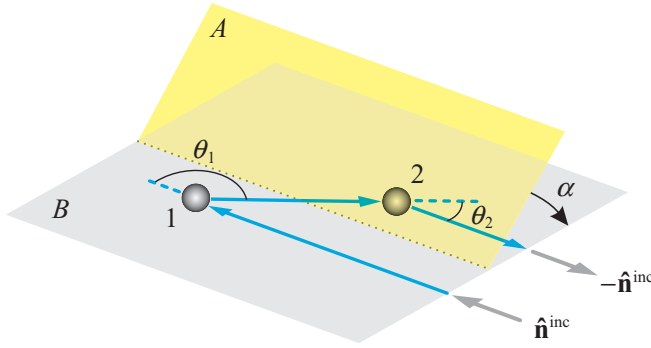


FIG. 2. (Color online) Second-order backscattering.

following matrix product:

$$\mathbf{M} = \mathbf{L}(\alpha)\mathbf{F}_2(\theta_2)\mathbf{F}_1(\theta_1)\mathbf{L}(\alpha). \quad (13)$$

Here,

$$\mathbf{L}(\eta) = \begin{pmatrix} 1 & 0 & 0 & 0 \\ 0 & \cos 2\eta & -\sin 2\eta & 0 \\ 0 & \sin 2\eta & \cos 2\eta & 0 \\ 0 & 0 & 0 & 1 \end{pmatrix} \quad (14)$$

is the rotation matrix describing the transformation of the Stokes parameters upon the rotation of the reference frame by an angle  $\eta$  in the clockwise sense as viewed in the direction of light propagation,  $\alpha$  is the angle between planes A and B,  $\mathbf{F}_i$  ( $i = 1, 2$ ) are the respective  $4 \times 4$  Stokes scattering matrices of particles 1 and 2 defined with respect to plane B, and  $\theta_i$  are the respective scattering angles (Fig. 2). Taking into account that for the spherical particles each scattering matrix is block-diagonal and has only four independent elements,

$$\mathbf{F}_i(\theta) = \begin{pmatrix} a_{i1}(\theta) & b_{i1}(\theta) & 0 & 0 \\ b_{i1}(\theta) & a_{i1}(\theta) & 0 & 0 \\ 0 & 0 & a_{i3}(\theta) & b_{i2}(\theta) \\ 0 & 0 & -b_{i2}(\theta) & a_{i3}(\theta) \end{pmatrix}, \quad (15)$$

one can easily verify that

$$M_{11} - M_{22} = -M_{33} + M_{44} \quad (16)$$

irrespective of  $\alpha$ . Obviously, this equality holds for any pair of particles and for any  $\hat{\mathbf{n}}^{\text{inc}}$ . Therefore, it also holds for the cumulative diffuse second-order scattering matrix,

$$\begin{aligned} R_{11}^2(-\hat{\mathbf{n}}^{\text{inc}}, \hat{\mathbf{n}}^{\text{inc}}) - R_{22}^2(-\hat{\mathbf{n}}^{\text{inc}}, \hat{\mathbf{n}}^{\text{inc}}) \\ = -R_{33}^2(-\hat{\mathbf{n}}^{\text{inc}}, \hat{\mathbf{n}}^{\text{inc}}) + R_{44}^2(-\hat{\mathbf{n}}^{\text{inc}}, \hat{\mathbf{n}}^{\text{inc}}). \end{aligned} \quad (17)$$

Upon substitution into Eqs. (11) and (17) obviously yields Eq. (12).

### III. NUMERICAL RESULTS

In the case of plane-parallel media consisting of sparsely distributed particles, the limits of Eq. (12) are well illustrated by the numerical results shown in Plate 14.6.3 and the left-hand bottom panel of Fig. 14.6.3 in [5]. In this section, we further demonstrate the second limit using direct computer solutions of the Maxwell equations for statistically homogeneous

spherical volumes of discrete random media following the general methodology described in [17].

Our model of discrete random media is a spherical volume randomly filled with  $N$  identical nonoverlapping spherical particles, as shown in Fig. 1. The dimension of the volume is specified in terms of its size parameter  $kR$ , where  $k$  is the wave number in the empty space surrounding the particles and  $R$  is the volume radius defined such that the corresponding sphere encloses the centers of all the constituent particles. The size of the particles is defined in terms of their size parameter  $ka$ , where  $a$  is the particle radius. The particle size parameter is fixed at  $ka = 2$ , while the particle refractive index is fixed at 1.31. The latter value is well representative of liquid water and water ice at visible wavelengths.

The multisphere volumes that are used in our computations were generated using a Monte Carlo algorithm designed to sequentially add spherical particles to a growing, enclosing spherical volume, in such a way so that the spheres do not overlap, and the distribution of spheres throughout the volume, at any point in the simulation, is statistically random with a uniform, set volume fraction  $f$ .

Each  $N$ -particle group thus configured is then used to average all far-field optical observables over the uniform orientation distribution of this configuration with respect to the laboratory reference frame. This approach yields, in effect, an infinite continuous set of random realizations of the spherical scattering volume and allows us to use the efficient analytical orientation averaging technique afforded by the superposition  $T$ -matrix method [18–20]. The latter represents a direct computer solver of the macroscopic Maxwell equations for a multisphere group. Within its range of numerical convergence, the corresponding  $T$ -matrix computer program generates results with a guaranteed number of accurate decimals, which makes this technique numerically exact. All calculations were performed using the most recent version of the multisphere  $T$ -matrix code described in [21]. This updated code is written in FORTRAN-90 in conjunction with message-passing interface (MPI) instructions and is designed to be run on distributed memory computer clusters.

As before, the overall scattering geometry is shown in Fig. 1. The incident light propagates in the direction  $\hat{\mathbf{n}}^{\text{inc}}$  and is scattered in the direction  $\hat{\mathbf{n}}^{\text{sca}}$ . The Stokes parameters of the incident and scattered light are specified with respect to the scattering plane, and the transformation of the Stokes parameters upon scattering is described by the respective far-field Mueller matrix  $\mathbf{R}$ . Since the multisphere configurations used are sufficiently “random” by design, averaging over all orientations of these configurations yields a block-diagonal Mueller matrix having only six independent significant elements,

$$\begin{pmatrix} I^{\text{sca}} \\ Q^{\text{sca}} \\ U^{\text{sca}} \\ V^{\text{sca}} \end{pmatrix} \propto \begin{pmatrix} R_{11}(\Theta) & R_{21}(\Theta) & 0 & 0 \\ R_{21}(\Theta) & R_{22}(\Theta) & 0 & 0 \\ 0 & 0 & R_{33}(\Theta) & R_{34}(\Theta) \\ 0 & 0 & -R_{34}(\Theta) & R_{44}(\Theta) \end{pmatrix} \times \begin{pmatrix} I^{\text{inc}} \\ Q^{\text{inc}} \\ U^{\text{inc}} \\ V^{\text{inc}} \end{pmatrix}. \quad (18)$$

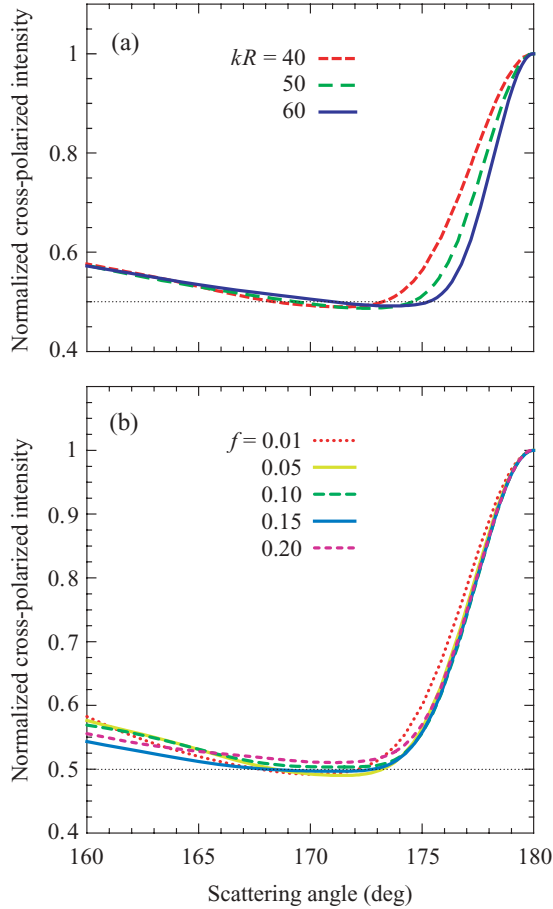


FIG. 3. (Color online) Normalized cross-polarized intensity vs scattering angle for spherically symmetric volumes of discrete random medium. (a) The volume packing density is fixed at  $f = 0.05$ . (b) The volume size parameter is fixed at  $kR = 40$ .

We found that in all the cases considered, the maximum magnitude of the matrix elements denoted by a zero does not exceed 0.001 that of the major elements.

Figure 3 depicts the angular distribution of the cross-polarized scattered intensity normalized by its backscattering value,

$$\frac{I_{\perp}^{\text{sca}}(\Theta)}{I_{\perp}^{\text{sca}}(180^{\circ})} = \frac{R_{11}(\Theta) - R_{22}(\Theta)}{R_{11}(180^{\circ}) - R_{22}(180^{\circ})}. \quad (19)$$

In panel (a), the packing density is fixed at  $f = 0.05$ , while  $kR$  is given values 40, 50, and 60 corresponding to  $N = 384, 752, \text{ and } 1301$ . In panel (b), the volume size parameter is fixed at  $kR = 40$ , while the packing density  $f$  is varied between 0.01 and 0.2. One can see that both panels exhibit pronounced backscattering peaks. The angular widths of the peaks scale as  $1/kR$  in panel (a) and are independent of  $f$  in panel (b), which is consistent with the CB origin of the peaks and relatively small optical thicknesses of the scattering volumes. The peaks are rounded at  $\Theta = 180^{\circ}$ , which is a typical trait of finite particulate media [22,23]. Finally, in agreement with the discussion in the previous section, the amplitudes of the cross-polarized intensity peaks are very close to 2.

#### IV. CONCLUDING REMARKS

The two limits of Eq. (12) supplement the set of general properties of CB characteristics of discrete random media composed of spherically symmetric particles as summarized in Sec. 14.5.5 of [5]. The very structure of the cross-polarized enhancement factor for spherical particles, wherein the first-order scattering contribution gets eliminated, endows  $\zeta_{\perp,\parallel}$  with a remarkable property of survival in circumstances when the majority of other manifestations of CB get strongly suppressed if not totally extinguished. This may make measurements of  $\zeta_{\perp,\parallel}$  a useful optical characterization tool in various physical, chemical, biomedical, engineering, and remote-sensing applications [24–28].

The apparent insensitivity of  $\zeta_{\perp,\parallel}$  to packing density revealed by Fig. 3(b) is intriguing. In fact, our computations for  $kR = 30$  (not shown) suggest that this invariance may hold up to packing densities  $\sim 0.4$ . Whereas the Lorenz-Mie values of the single-particle extinction cross section may be applicable to sparsely distributed particles with  $f = 0.01$ , they become quite questionable in application to densely packed particles with  $f \geq 0.05$ . In this regard, Fig. 3(b) may be indicative of a substantial decrease of the single-particle extinction cross section with increasing  $f$  which results in comparable values of the respective optical diameters of the five scattering volumes despite a 20-fold variation of the packing density.

The general property (17) of the diffuse second-order backscattering Mueller matrix may have important implications for active remote sensing of liquid-droplet clouds in the terrestrial atmosphere. Indeed, exactly the same property is possessed by the Mueller matrix describing first-order backscattering from nonspherical particles [see Eq. (2.131) of [15]]. This implies that a nonzero contribution of multiple scattering to the lidar or radar signal can easily be misinterpreted in terms of the presence of nonspherical particles. Averaging over all  $\alpha$  in Fig. 2 yields

$$R_{22}^2(-\hat{\mathbf{n}}^{\text{inc}}, \hat{\mathbf{n}}^{\text{inc}}) = -R_{33}^2(-\hat{\mathbf{n}}^{\text{inc}}, \hat{\mathbf{n}}^{\text{inc}}), \quad (20)$$

which exacerbates the problem even further by implying the standard “nonspherical” relationship between the resulting linear and circular depolarization ratios [see Eq. (10.4) of [15]].

Finally, we note that while Eq. (12) represents a noteworthy result for classical scatterers considered in this paper, similar limits have been obtained previously for the case of cold atomic media [29–31]. In particular, the cross-polarized enhancement factor of 2 for double scattering by cold strontium atoms has been reported based on both experimental and theoretical studies [32], which may reveal an interesting analogy between quantum and spherically symmetric classical scatterers.

#### ACKNOWLEDGMENTS

We thank the anonymous reviewer for an instructive suggestion. This research was supported in part by the NASA Radiation Sciences Program managed by Hal Maring.

- [1] L. Tsang, J. A. Kong, and R. T. Shin, *Theory of Microwave Remote Sensing* (Wiley, New York, 1985).
- [2] Y. N. Barabanenkov, Yu. A. Kravtsov, V. D. Ozhin, and A. Saichev, *Prog. Opt.* **29**, 65 (1991).
- [3] *Wave Scattering in Complex Media: From Theory to Applications*, edited by B. van Tiggelen and S. E. Skipetrov (Kluwer, Dordrecht, The Netherlands, 2003).
- [4] P. Sheng, *Introduction to Wave Scattering, Localization and Mesoscopic Phenomena* (Springer, Berlin, 2006).
- [5] M. I. Mishchenko, L. D. Travis, and A. A. Lacis, *Multiple Scattering of Light by Particles: Radiative Transfer and Coherent Backscattering* (Cambridge University Press, Cambridge, 2006).
- [6] E. Akkermans and G. Montambaux, *Mesoscopic Physics of Electrons and Photons* (Cambridge University Press, Cambridge, 2007).
- [7] M. P. van Albada, M. B. van der Mark, and A. Lagendijk, *J. Phys. D* **21**, S28 (1988).
- [8] P. E. Wolf, G. Maret, E. Akkermans, and R. Maynard, *J. Phys. (France)* **49**, 63 (1988).
- [9] Y. N. Gnedin and A. Z. Dolginov, *Sov. Phys. JETP* **18**, 784 (1964).
- [10] K. M. Watson, *J. Math. Phys.* **10**, 688 (1969).
- [11] Y. N. Barabanenkov, *Radiophys. Quant. Electron.* **16**, 65 (1973).
- [12] L. Tsang and A. Ishimaru, *J. Opt. Soc. Am. A* **1**, 836 (1984).
- [13] M. P. Van Albada and A. Lagendijk, *Phys. Rev. Lett.* **55**, 2692 (1985).
- [14] P.-E. Wolf and G. Maret, *Phys. Rev. Lett.* **55**, 2696 (1985).
- [15] M. I. Mishchenko, L. D. Travis, and A. A. Lacis, *Scattering, Absorption, and Emission of Light by Small Particles* (Cambridge University Press, Cambridge, 2002) [<http://www.giss.nasa.gov/staff/mmishchenko/books.html>].
- [16] M. I. Mishchenko, *J. Opt. Soc. Am. A* **9**, 978 (1992).
- [17] M. I. Mishchenko, L. Liu, D. W. Mackowski, B. Cairns, and G. Videen, *Opt. Express* **15**, 2822 (2007).
- [18] D. W. Mackowski, *J. Opt. Soc. Am. A* **11**, 2851 (1994).
- [19] M. I. Mishchenko and D. W. Mackowski, *Opt. Lett.* **19**, 1604 (1994).
- [20] D. W. Mackowski and M. I. Mishchenko, *J. Opt. Soc. Am. A* **13**, 2266 (1996).
- [21] D. W. Mackowski, *J. Quant. Spectrosc. Radiat. Transf.* **70**, 441 (2001).
- [22] S. Etemad, R. Thompson, M. J. Andrejco, S. John, and F. C. MacKintosh, *Phys. Rev. Lett.* **59**, 1420 (1987).
- [23] K. Muinonen, *Waves Random Media* **14**, 365 (2004).
- [24] *Scattering in Polymetric and Colloidal Systems*, edited by W. Brown and K. Mortensen (Gordon and Breach, Amsterdam, 2000).
- [25] V. V. Tuchin, L. V. Wang, and D. A. Zimnyakov, *Optical Polarization in Biomedical Applications* (Springer, Berlin, 2006).
- [26] V. Tuchin, *Tissue Optics* (SPIE, Bellingham, WA, 2007).
- [27] *Photopolarimetry in Remote Sensing*, edited by G. Videen, Y. Yatskiv, and M. Mishchenko (Kluwer, Dordrecht, 2004).
- [28] M. I. Mishchenko, V. K. Rosenbush, N. N. Kiselev, D. F. Lupishko, V. P. Tishkovets, V. G. Kaydash, I. N. Belskaya, Y. S. Efimov, and N. M. Shakhovskoy, *Polarimetric Remote Sensing of Solar System Objects* (Akad., Kyiv, 2010). [arXiv:1010.1171](https://arxiv.org/abs/1010.1171)
- [29] G. Labeyrie, F. de Tomasi, J.-C. Bernard, C. A. Müller, Ch. Miniatura, and R. Kaiser, *Phys. Rev. Lett.* **83**, 5266 (1999).
- [30] G. Labeyrie, C. A. Müller, D. S. Wiersma, Ch. Miniatura, and R. Kaiser, *J. Opt. B* **2**, 672 (2000).
- [31] C. A. Müller, T. Jonckheere, Ch. Miniatura, and D. Delande, *Phys. Rev. A* **64**, 053804 (2001).
- [32] Y. Bidet, B. Klappauf, J. C. Bernard, D. Delande, G. Labeyrie, Ch. Miniatura, D. Wilkowski, and R. Kaiser, *Phys. Rev. Lett.* **88**, 203902 (2002).